Erratum

Measurement of $D^{*\pm}$ production and the charm contribution to F_2 in deep inelastic scattering at HERA

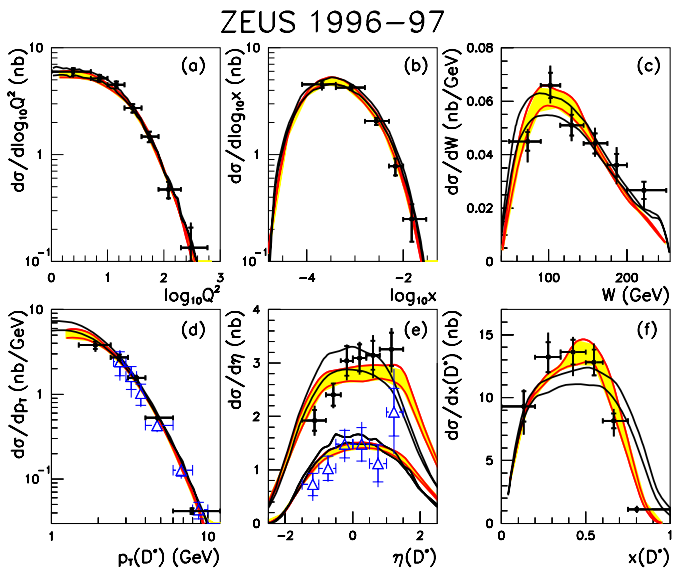The ZEUS Collaboration

After the online-first and print publication we discovered errors in Fig. 5 and Tables 1, 2, 3. The correct figure and tables should read as follows.

Fig. 5a–f. Differential cross sections for $D^{*\pm}$ production from the $K2\pi$ final state (solid dots) in the Q^2, y, $p_T(D^*)$ and $\eta(D^*)$ kinematic region as functions of **a** $\log_{10} Q^2$, **b** $\log_{10} x$, **c** W, **d** $p_T(D^*)$, **e** $\eta(D^*)$ and **f** $x(D^*)$. The inner error bars show the statistical uncertainties while the outer ones show the statistical and systematic uncertainties summed in quadrature. The results from the $K4\pi$ channel (open triangles) are also shown in the $p_T(D^*)$**d** and $\eta(D^*)$ **e** plots. The data are compared with the NLO QCD calculation as implemented in HVQDIS using the ZEUS NLO pdf's. The open band corresponds to the standard Peterson fragmentation function with the parameter $\epsilon = 0.035$. For the shaded band, the Peterson fragmentation was replaced by that extracted from RAPGAP (see the text for details). The boundaries of the bands correspond to charm mass variations between 1.3 (upper curve) and 1.5 GeV(lower curve). In **a** and **b**, the open band is indistinguishable from the shaded band

Table 1. The $D^* \to K\pi\pi_s$ and $D^* \to K\pi\pi\pi_s$ differential cross sections. The bin range, the center-of-gravity of the bin (see text) and the cross sections for all the data in Figs. 5 and 6 are shown. The first error is the statistical error and the asymmetric errors are the statistical and systematic uncertainties added in quadrature. The overall normalization uncertainties arising from the luminosity measurement ($\pm1.65\%$) and from the $D^{*\pm}$ and D^0 decay branching ratios are not included

$K\pi\pi_s$		$K\pi\pi_s$	
(range) $log_{10}(Q^2)$	$d\sigma/dlog_{10}(Q^2)$ (nb)	(range) $log_{10}(x)$	$d\sigma/dlog_{10}(x)$ (nb)
(0.0,0.7) 0.39	$5.99\pm0.47\ ^{+0.61}_{-0.74}$	(-4.1,-3.4) -3.69	$4.54 \pm 0.35\ ^{+0.45}_{-0.56}$
(0.7,1.0) 0.85	$5.17\pm0.39\ ^{+0.54}_{-0.46}$	(-3.4,-2.8) -3.08	$4.24 \pm 0.23\ ^{+0.34}_{-0.27}$
(1.0,1.3) 1.16	$4.50\pm0.33\ ^{+0.43}_{-0.44}$	(-2.8,-2.3) -2.56	$2.06 \pm 0.16\ ^{+0.19}_{-0.17}$
(1.3,1.6) 1.45	$2.72\pm0.25\ ^{+0.32}_{-0.29}$	(-2.3,-2.0) -2.16	$0.78 \pm 0.14\ ^{+0.15}_{-0.16}$
(1.6,1.9) 1.74	$1.47\pm0.17\ ^{+0.18}_{-0.17}$	(-2.0,-1.5) -1.82	$0.25 \pm 0.10\ ^{+0.11}_{-0.10}$
(1.9,2.3) 2.08	$0.47\pm0.08\ ^{+0.11}_{-0.10}$		
(2.3,2.8) 2.48	$0.135\pm0.073\ ^{+0.096}_{-0.073}$		

$K\pi\pi_s$		$K\pi\pi_s$	
(range) W (GeV)	$d\sigma/dW$ (nb/GeV)	(range) $x(D^*)$	$d\sigma/dx(D^*)$ (nb)
(50,90) 73	$0.0450\pm0.0035^{+0.0047}_{-0.0079}$	(0.0,0.2) 0.13	$9.3 \pm 1.2\ ^{+1.4}_{-2.2}$
(90,115) 102	$0.0659\pm0.0048^{+0.0074}_{-0.0068}$	(0.2,0.35) 0.28	$13.2 \pm 1.2\ ^{+1.9}_{-1.4}$
(115,145) 129	$0.0510\pm0.0039^{+0.0068}_{-0.0059}$	(0.35,0.5) 0.42	$13.61 \pm 0.98\ ^{+1.22}_{-1.90}$
(145,175) 159	$0.0442\pm0.0038^{+0.0059}_{-0.0049}$	(0.5,0.6) 0.55	$12.79 \pm 1.03\ ^{+1.49}_{-1.03}$
(175,200) 187	$0.0361\pm0.0043^{+0.0067}_{-0.0071}$	(0.6,0.75) 0.67	$8.15 \pm 0.60\ ^{+0.95}_{-1.24}$
(200,250) 222	$0.0266\pm0.0032^{+0.0033}_{-0.0069}$	(0.75,1.0) 0.80	$1.12 \pm 0.10\ ^{+0.27}_{-0.27}$

$K\pi\pi_s$		$K\pi\pi\pi_s$	
(range) $p_T(D^*)$ (GeV)	$d\sigma/dp_T(D^*)$ (nb/GeV)	(range) $p_T(D^*)$ (GeV)	$d\sigma/dp_T(D^*)$ (nb/GeV)
(1.5,2.4) 1.91	$3.82\pm0.39\ ^{+0.48}_{-0.65}$	(2.5,3.0) 2.74	$2.42 \pm 0.76\ ^{+0.90}_{-0.97}$
(2.4,3.1) 2.72	$2.72\pm0.21\ ^{+0.26}_{-0.28}$	(3.0,3.5) 3.24	$1.63 \pm 0.49\ ^{+0.52}_{-0.71}$
(3.1,4.0) 3.50	$1.57\pm0.10\ ^{+0.14}_{-0.13}$	(3.5,4.0) 3.73	$1.03 \pm 0.29\ ^{+0.31}_{-0.33}$
(4.0,6.0) 4.77	$0.527\pm0.033\ ^{+0.041}_{-0.047}$	(4.0,6.0) 4.74	$0.43 \pm 0.06\ ^{+0.07}_{-0.07}$
(6.0,15.0) 7.93	$0.0419\pm0.0034^{+0.0043}_{-0.0041}$	(6.0,8.0) 6.77	$0.127 \pm 0.019^{+0.022}_{-0.026}$
		(8.0,10.0) 8.75	$0.044 \pm 0.010^{+0.011}_{-0.010}$
		(10.0,15.0) 11.73	$0.007 \pm 0.002^{+0.003}_{-0.003}$

$K\pi\pi_s$		$K\pi\pi\pi_s$	
(range) $\eta(D^*)$	$d\sigma/d\eta(D^*)$ (nb)	(range) $\eta(D^*)$	$d\sigma/d\eta(D^*)$ (nb)
(-1.5,-0.8) -1.13	$1.93\pm0.19\ ^{+0.27}_{-0.29}$	(-1.5,-1.0) -1.18	$0.73 \pm 0.21\ ^{+0.22}_{-0.31}$
(-0.8,-0.35) -0.58	$2.41\pm0.21\ ^{+0.22}_{-0.25}$	(-1.0,-0.5) -0.73	$1.03 \pm 0.23\ ^{+0.25}_{-0.25}$
(-0.35,0.0) -0.18	$3.04\pm0.28\ ^{+0.30}_{-0.37}$	(-0.5,0.0) -0.24	$1.48 \pm 0.26\ ^{+0.29}_{-0.34}$
(0.0,0.4) 0.20	$3.09\pm0.25\ ^{+0.30}_{-0.31}$	(0.0,0.5) 0.26	$1.48 \pm 0.31\ ^{+0.42}_{-0.33}$
(0.4,0.8) 0.60	$3.15\pm0.27\ ^{+0.38}_{-0.43}$	(0.5,1.0) 0.75	$1.12 \pm 0.35\ ^{+0.36}_{-0.44}$
(0.8,1.5) 1.15	$3.26\pm0.31\ ^{+0.40}_{-0.44}$	(1.0,1.5) 1.22	$2.08 \pm 0.45\ ^{+0.81}_{-0.78}$

Table 2. The cross sections for $D^{*\pm}$ production from the $K2\pi$ final state. The table contains for each bin: the Q^2 range of the bin; the y range of the bin; the measured $D^{*\pm}$ cross section in the bin with statistical and systematic uncertainties; and the HVQDIS prediction for this cross section. The overall normalization uncertainties arising from the luminosity measurement ($\pm1.65\%$) and from the $D^{*\pm}$ and D^0 decay branching ratios are not included

Q^2 range (GeV^2)	y range	$\sigma(D^*)$ meas. (nb)	$\sigma(D^*)$ pred.(nb)
1–3.5	0.70–0.24	$1.45 \pm 0.23^{+0.20}_{-0.22}$	1.12
	0.24–0.11	$1.00 \pm 0.20^{+0.17}_{-0.17}$	1.00
	0.11–0.02	$0.92 \pm 0.16^{+0.15}_{-0.09}$	1.10
3.5–6.5	0.70–0.22	$0.73 \pm 0.10^{+0.07}_{-0.11}$	0.54
	0.22–0.11	$0.342 \pm 0.055^{+0.068}_{-0.036}$	0.405
	0.11–0.02	$0.433 \pm 0.066^{+0.069}_{-0.076}$	0.528
6.5–9	0.70–0.15	$0.388 \pm 0.060^{+0.051}_{-0.053}$	0.369
	0.15–0.02	$0.288 \pm 0.046^{+0.068}_{-0.008}$	0.355
9–14	0.70–0.23	$0.370 \pm 0.057^{+0.038}_{-0.030}$	0.302
	0.23–0.11	$0.314 \pm 0.045^{+0.051}_{-0.076}$	0.251
	0.11–0.02	$0.253 \pm 0.042^{+0.011}_{-0.020}$	0.316
14–22	0.70–0.23	$0.25 \pm 0.05^{+0.11}_{-0.02}$	0.26
	0.23–0.11	$0.254 \pm 0.043^{+0.044}_{-0.073}$	0.212
	0.11–0.02	$0.226 \pm 0.035^{+0.052}_{-0.027}$	0.250
22–44	0.70–0.23	$0.387 \pm 0.053^{+0.052}_{-0.040}$	0.301
	0.23–0.11	$0.200 \pm 0.027^{+0.028}_{-0.021}$	0.226
	0.11–0.02	$0.198 \pm 0.033^{+0.031}_{-0.018}$	0.240
44–90	0.70–0.23	$0.202 \pm 0.043^{+0.050}_{-0.019}$	0.188
	0.23–0.02	$0.200 \pm 0.032^{+0.011}_{-0.016}$	0.221
90–200	0.70–0.23	$0.090 \pm 0.023^{+0.009}_{-0.013}$	0.099
	0.23–0.02	$0.075 \pm 0.015^{+0.010}_{-0.007}$	0.086

Table 3. The cross sections for $D^{*\pm}$ production from the $K4\pi$ final state. The table contains for each bin: the Q^2 range of the bin; the y range of the bin; the measured $D^{*\pm}$ cross section in the bin with statistical and systematic uncertainties; and the HVQDIS prediction for this cross section. The overall normalization uncertainties arising from the luminosity measurement ($\pm1.65\%$) and from the $D^{*\pm}$ and D^0 decay branching ratios are not included

Q^2 range (GeV^2)	y range	$\sigma(D^*)$ meas. (nb)	$\sigma(D^*)$ pred. (nb)
1–10	0.70–0.34	$0.94\pm0.29^{+0.39}_{-0.21}$	0.61
	0.34–0.02	$1.39\pm0.51^{+0.21}_{-0.09}$	1.55
10–21	0.70–0.28	$0.35\pm0.08^{+0.11}_{-0.06}$	0.21
	0.28–0.02	$0.59\pm0.11^{+0.07}_{-0.11}$	0.47
21–33	0.70–0.22	$0.115\pm0.055^{+0.039}_{-0.023}$	0.154
	0.22–0.02	$0.125\pm0.045^{+0.048}_{-0.050}$	0.209
50–600	0.70–0.22	$0.23\pm0.07^{+0.07}_{-0.13}$	0.249
	0.22–0.02	$0.240\pm0.061^{+0.059}_{-0.084}$	0.221